RESEARCH

Effect of manganese on the structure of CMAS slag glass–ceramics

Rui Ma[1,2] · YuXuan Zhang[1,2] · ShunLi OuYang[1,2] · NanNan Wu[2] · Yang Li[2]

Abstract

With the acceleration of industrialization, environmental issues have received great attention from governments and societies around the world. Utilizing solid wastes containing valuable heavy metals and exploring their role and application in materials is one of the focal issues of environmental protection in recent years. In this paper, in order to explore the effect of Mn content on the crystallization of CaO-MgO-Al_2O_3-SiO_2 glass–ceramics, glass–ceramics with different content of MnO_2 were prepared by sintering method and the effect of MnO_2 doping on the crystalline properties, glass stability and heavy metal fixation properties of the stainless steel slag glass–ceramics was investigated by differential scanning calorimetry (DSC), Raman spectroscopy, X-ray diffraction (XRD) and scanning electron microscope (SEM). The analysis using crystallization kinetics showed that surface crystallization dominated the whole crystallization process in the range of 0% to 10% MnO_2 content. The peak glass crystallization and depolymerisation temperatures of the glass–ceramics increased gradually with increasing MnO_2 content, and the main crystallization mode of the samples was one-dimensional crystallization. The main crystalline phase of the resulting glass–ceramics was transformed from diopside to spinel, with a crystallization temperature of 860℃. Heavy metals solidified in the spinel phase. This study shows that heavy metals can be effectively immobilized in glass–ceramics. In summary, the use of solid waste to prepare final products with good environmental performance provides a feasible way to utilize solid waste resources.

Keywords Stainless steel slag glass–ceramics · MnO_2 · Heavy metals · Immobilization · Raman spectroscopy

Introduction

In recent years, the rapid economic and industrial development of China has led to a sharp increase in the generation of solid waste and increasingly serious environmental pollution. A variety of high-risk heavy metal elements exist in solid waste, threatening human health and the natural environment. According to statistics, from 2014 to 2018, the annual generation of municipal industrial hazardous waste in China increased at a rate of 15% to 21%.In 2018, the generation of industrial hazardous waste in 200 cities reached 4,643 million tonnes [1]. One of the urgent needs of countries to

develop without causing large-scale environmental and health problems is how to dispose of high-risk solid waste in an environmentally sound manner [2]. Currently, the most commonly used methods for mitigating hazardous metal contamination in solid wastes include thermochemical treatment [3, 4], solvent extraction [5, 6], adsorption [7, 8] and bioleaching [9]. However, the risk of re-dissolution of heavy metals is present in all of these treatment methods, which cannot achieve the desired results. Therefore, it is crucial to solve the problem of resourceful utilization and harmless treatment of solid wastes. Glass–ceramics is a material consisting of a glassy phase and a crystalline phase formed by controlling the crystallization of the base glass. Glass ceramics have excellent mechanical properties and can also be used for detoxification and immobilization of heavy metals in waste [10]. Liu et al. [11] prepared glass–ceramics using amorphous slag of oil shale ash and studied the existence of heavy metal elements Pb and Cu in glass–ceramics. The results show that PbO is not stable in the glass–ceramics, and Pb is more easily solidified in the glass matrix in an amorphous state, while Cu is more inclined to exist in the

✉ ShunLi OuYang
  ouyangshunli01@163.com

✉ NanNan Wu
  woshinannan04@163.com

1   School of Material and Metallurgy, Inner Mongolia University of Science and Technology, Baotou 014010, China

2   Guangzhou Maritime University, Guangzhou 510725, China

form of CuO in the glass–ceramics. Pan et al. [12] prepared glass–ceramics from smoked lead slag, and found that heavy metal ions Pb^{2+}, Zn^{2+} and Cd^{2+} can be solidified in the glass phase or crystal phase, in which Pb^{2+} mainly exists in the glass matrix in the form of lead-oxygen tetrahedron structure. Zn^{2+}; because the radius of Fe^{2+} is close to the radius of Fe^{2+} ion, it can enter the crystal structure of calcium iron pyroxene by substitution. Therefore, glass–ceramic preparation technology has been widely used for the environmentally sound treatment and resource utilization of solid waste.

Currently, various solid wastes, such as dismantled waste batteries, ferrochrome slag, medical waste incineration ash and other hazardous waste incineration residues, have been proven to be effectively immobilized by glass–ceramics [13–15]. In general, the effectiveness of glass–ceramics in immobilized hazardous metals is closely related to the structure of the glass–ceramics, which is mainly determined by its basic composition and crystallization behaviour.In recent years, Mn-doped glass- ceramics have gradually attracted attention. Dai et al. [16] found through experiments that Mn ions improved the crystallization ability of glass–ceramics by destroying the glass network structure, thereby enhancing the mechanical properties of glass–ceramics. The Mn ions has a significant modification effect on the glass network structure. Abdel-Hameed et al. [17] studied the effect of P_2O_5 and MnO_2 on the crystallization behavior of magnetic glass–ceramics in the Fe_2O_3-ZnO-CaO-SiO_2-B_2O_3 system. Cooling from melting temperature The addition of MnO_2 increases the formation of magnetite phase. The M_S value reached 58.99 emu/g. Wang et al. [18] found that the increase of MnO_2 at room temperature will lead to the dielectric properties of barium strontium titanate glass–ceramics by preparing barium strontium titanate glass ceramics. However, few reports have described the effects of Mn-doped glass–ceramics on their crystallization behaviour.

In this paper, we use different heating rates to test the samples by DSC, and determine the heat treatment system and crystallization activation energy of the samples by DSC curves of different heating rates, so as to analyze the crystallization behavior of glass–ceramics more accurately. And glass–ceramics containing heavy metal manganese were prepared by melting method and the crystallization kinetics

and glass stability of the glass samples were investigated by DSC. Meanwhile, the properties of the glass samples and the structure of the glass–ceramics containing manganese slag were observed by XRD and SEM. The results of the study provide a theoretical basis for the effective use of manganese-containing slag.

Materials and methods

Chemicals

Fly ash, stainless steel slag from a steel plant in Baotou, quartz sand, CaO, MgO, B_2O_5 from a national pharmaceutical plant.

Preparation of experimental samples

Composition of the base glasses with different MnO_2 contents is shown in Table 1 (wt%).

Stainless steel slag (SSS) is a suitable starting material for the preparation of CaO-MgO-Al_2O_3-SiO_2 (CMAS) glass–ceramics [19, 20]. Therefore, CMAS glass–ceramics with different MnO_2 ratios were designed in the present experiments based on the introduction of fly ash with stainless steel slag.

The designed parent glasses and their sample numbers are listed in Table 1. Quartz sand (> 99 mass %), calcium oxide (> 99 mass %), magnesium oxide (> 99 mass %), and borax (> 99 mass %) reagents were used in the experiments to supplement make up for the lack of the main components of the CMAS glass. According to the designed recipe, 188 g of ingredients were weighed and then mixed in a ball mill for 2 h.

A homogeneous mixture was obtained. Each quartz crucible containing the homogeneous mixture was melted in a high temperature chamber resistance furnace at 1550 °C for 3 h. Approximately 5% of each molten specimen is poured in water and these water quenched specimens are used for DSC analysis. The residual molten glass is formed in a metal mould and annealed to obtain the basic glass. Glass samples

Table 1 Base glass composition

	MnO_2	Fly ash	Stainless steel slag	SiO_2	CaO	MgO	B_2O_5	Total
M1	0	67.4	16.9	4.4	5.2	0.9	5.2	100
M2	2	66.1	16.5	4.3	5.1	0.9	5.1	100
M3	4	64.8	16.2	4.2	5.0	0.8	5.0	100
M4	6	63.5	15.8	4.1	4.9	0.8	4.9	100
M5	8	62.1	15.5	4.0	4.8	0.8	4.8	100
M6	10	60.7	15.2	3.9	4.7	0.8	4.7	100

are prepared by DSC analysis to determine the appropriate crystallization temperature under heating conditions.

Material characterisation

A differential thermal analyser (NETZSCH STA 449C) was used to obtain the precipitation peak temperature (T_p) of the crystallization glass, which was heated at rates of 5, 10, 15, and 20 °C/min over the temperature range of 25℃ to 1300℃. The kinetic behaviour of the glass was investigated in an argon atmosphere. An X-ray diffractometer (Panalytical X'pert Pro Powder) is used to analyze the physical phase of glass–ceramics samples with a scanning angular speed of 0.2º/s and a scanning angle range of 10º to 80º. The Zeiss Supra 55 FESEM was used to analyse the microstructure and organisation of the glass–ceramics samples, which were cut into small rectangles of 3 mm×4 mm×6 mm, with a flat surface where defects (e.g. porosity) were not visible to the naked eye, and then abraded with 600 to 2000 grit metallographic paper. Rough grinding step by step. Then on a polishing machine, choose a 0.25 µm diamond spray polish and polish until the surface is free of scratches and appears as a mirror surface. The surface was then etched with a 5% HF acid solution for 70 s, followed by rinsing off the residual acid from the eroded surface with distilled water and ethanol, drying with a hairdryer and then fixing the microcrystalline glass sample on a carrier table with conductive adhesive and plating with a metal conductive film using an ion jetting instrument; The Raman spectrometer (Renishaw-inVia) was used for the structural determination of samples, equipped with an automated x—y—z stage, 50×Olympus teleobjective with a resolution of ±1 cm^{-1}, 532 nm laser wavelength, 1800 lines/mm grating, exposure time of 3 s, 2 accumulations, and a scanning waveform in the range of 100 to 1900 cm^{-1}, and all spectra were collected at room temperature.

Results and Discussion

Crystallization kinetic calculations

Glass–ceramics melt from the glass state to the crystalline state, the need to have a certain activation energy to overcome the structural unit rearrangement of the energy barrier, this activation energy that is the crystallization activation energy. The lower the potential barrier, the smaller the activation energy required for precipitation, the easier it is to precipitate the glass, so it is very important to calculate the crystallization activation energy in the crystallization process.

The resulting melt was quenched quickly in water to prevent crystallization, and the resulting sample was crushed and sieved through a 200 mesh sieve to make it suitable for DSC testing. The samples were heated at different rates of 5, 10, 15, and 20 °C min^{-1} from 25 °C to 1300 °C, respectively. The DSC data shown in Fig. 1.

On the basis of DSC data such as crystallization temperature (T_c), crystallization onset temperature (T_o) and glass transition temperature (T_g), the glass stability parameter K_{GS} was calculated as follows [21, 22]:

$$\Delta T = T_o - T_g \tag{1}$$

$$K_{GS} = \Delta T(T_c - T_g)/T_g \tag{2}$$

It can according to the crystallization kinetic theory proposed by Kissinger [23] and the crystallization kinetic theory proposed by Augis-Bennett [24]. The Avrami index n reflects the complexity of the phase transition. When n = 1, the phase transition process is a first-order reaction, that is, the transition rate is proportional to the concentration of the reactants. When n = 2, the phase transition process is a second-order reaction, that is, the transition rate is proportional to the square of the concentration of the reactants. When n > 2, the phase transition process is a complex multistage reaction. The crystallization activation energy (E_c) and Avrami index (n) can be determined as follows

$$\ln\frac{T_p{}^2}{\alpha} = \frac{E}{RT_p} + \ln\frac{E}{R} \tag{3}$$

$$n = \frac{2.5RT_c^2}{T_H \times E_c} \tag{4}$$

where α, R, T_H and T_C are the heating rate, ideal gas constant, exothermic peak half-peak width and crystallization temperature corresponding to different α values for the DSC test respectively.

Using the Kissinger method to calculate the crystallization activation energy, Kissinger introduced the equation for the relationship between the peak temperature of glass precipitation, T_p, and the rate of temperature increase, α, analyzed by the DSC test [25]:

$$\ln\frac{T_p{}^2}{\alpha} = \frac{E_1}{RT_p} + \ln\frac{E_1}{R} - \ln\nu \tag{5}$$

where α is the rate of temperature rise for the DSC test analysis, T_P is the temperature of the exothermic peak of precipitation on the DSC test analysis curve; ν and is the frequency factor. A curve of $\ln\left(\frac{T_p^2}{\alpha}\right)$ versus $\frac{1}{T_p}$ with a slope of $\frac{E_1}{R}$ and an $\ln\left(\frac{T_p^2}{\alpha}\right)$ axis intercept of $\ln\left(\frac{E_1}{R}\right) - \ln\nu$ gives the crystallization activation energy under the Kissinger formula E_1.

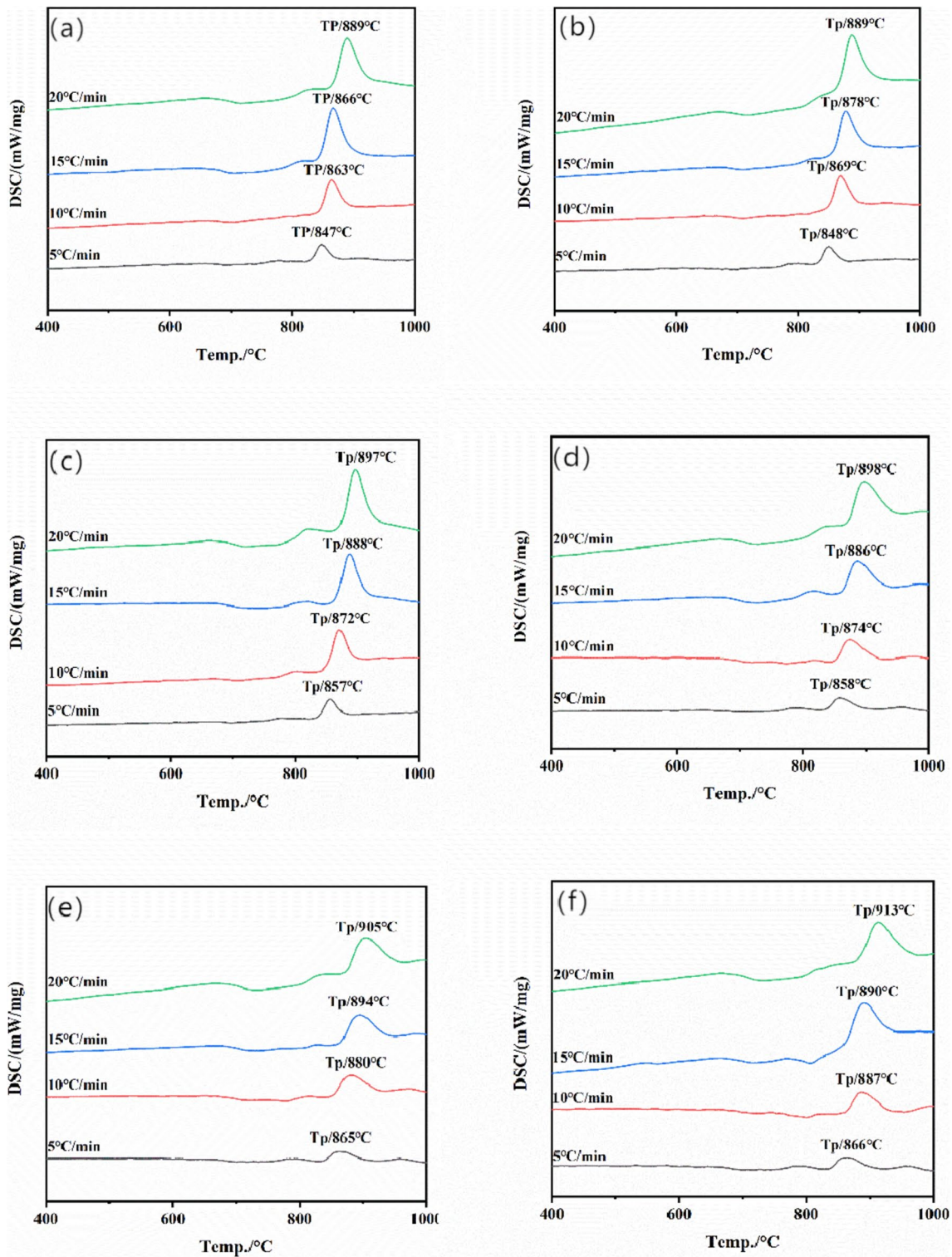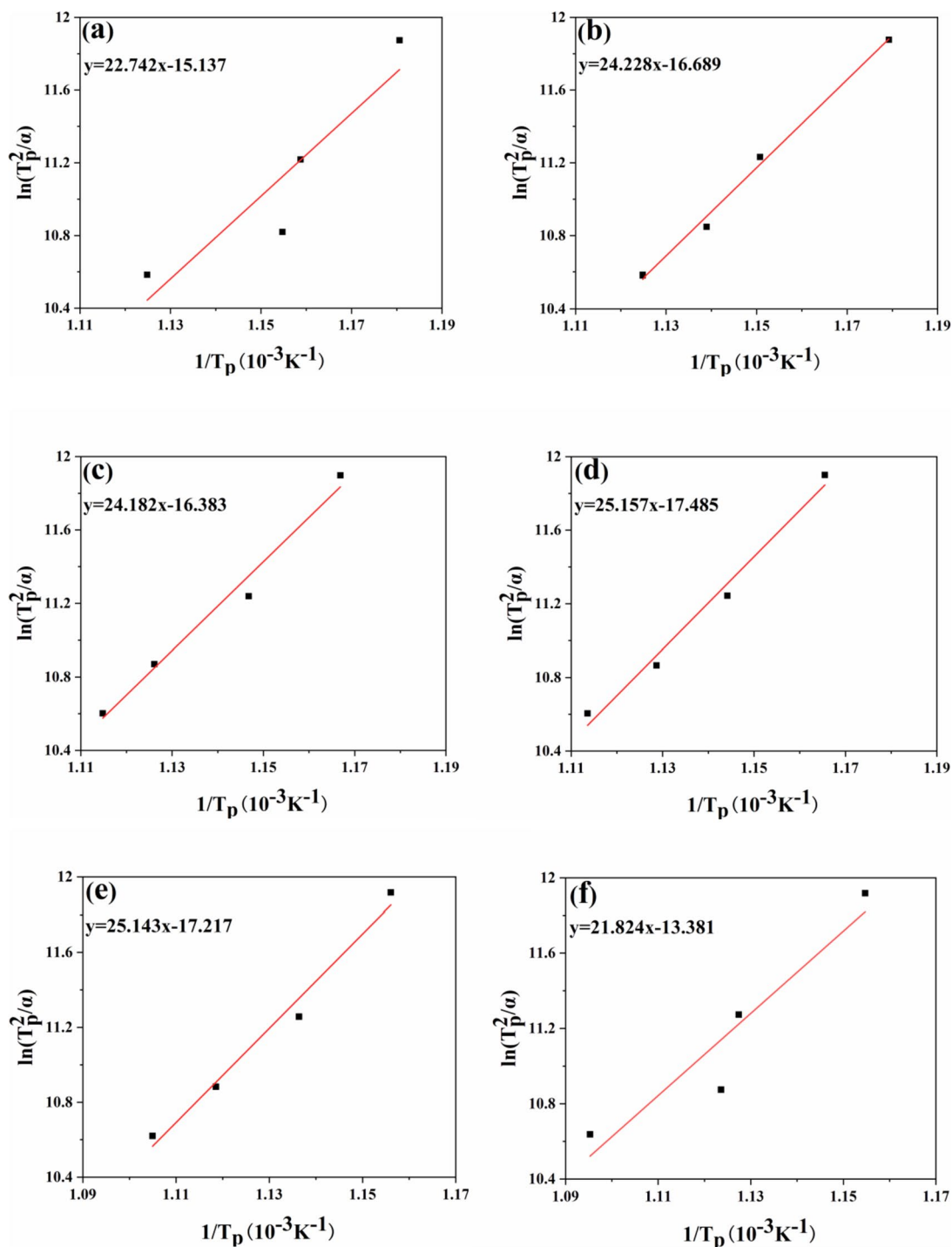**Fig. 1** DSC curves (a–f) of glass–ceramics with different MnO_2-doping: a: 0, b: 2%, c: 4%, d: 6%, e: 8%, f:10%

According to Kissinger, a straight line was fitted to the different glass–ceramics, and the results of the fit are shown in Fig. 2.

Similarly, the crystallization activation energy can be calculated using the Owaza method, where Owaza's relation is given by

Fig. 2 $\ln(T_p^2/\alpha)$ vs. $1/T_p$ of glasses with different MnO_2-doping (a-f): a: 0, b: 2%, c: 4%, d: 6%, e: 8%, f:10%.

$$\ln\alpha = -\frac{E_2}{RT_p} + C_1 \tag{6}$$

where α is the DSC test analysis heating rate, T_P is the temperature of the exothermic peak of crystallization on the DSC test analysis curve; and C_1 is a constant. making a curve fitting $-\ln\alpha$ to $\frac{1}{T_p}$, the slope of the curve is $\frac{E_2}{R}$, which gives the crystallization activation energy E_2 under the Owaza formula.

According to the Owaza equation, a straight line was fitted to the different glass–ceramics and the results obtained from the fit are shown in Fig. 3.

Each sample showed a single crystallization peak temperature between 840℃ and 920℃ at different heating rates, as shown in Fig. 3. The crystallization temperatures of the samples first increased and then stabilized as the doping amount of MnO_2 increased. Zhang et al. [26]

prepared glass–ceramics using electrolytic manganese slag as raw material. It is found that Mn ions form Mn–O tetrahedron by substituting Al or Si ions. Thus, Mn is a network former that is able to enter into the silica-oxygen network in the form of $[MnO_4]$ when added to the glass. On the one hand, MnO_2 changes the connectivity of the glass network and increases the stability of the glass; on
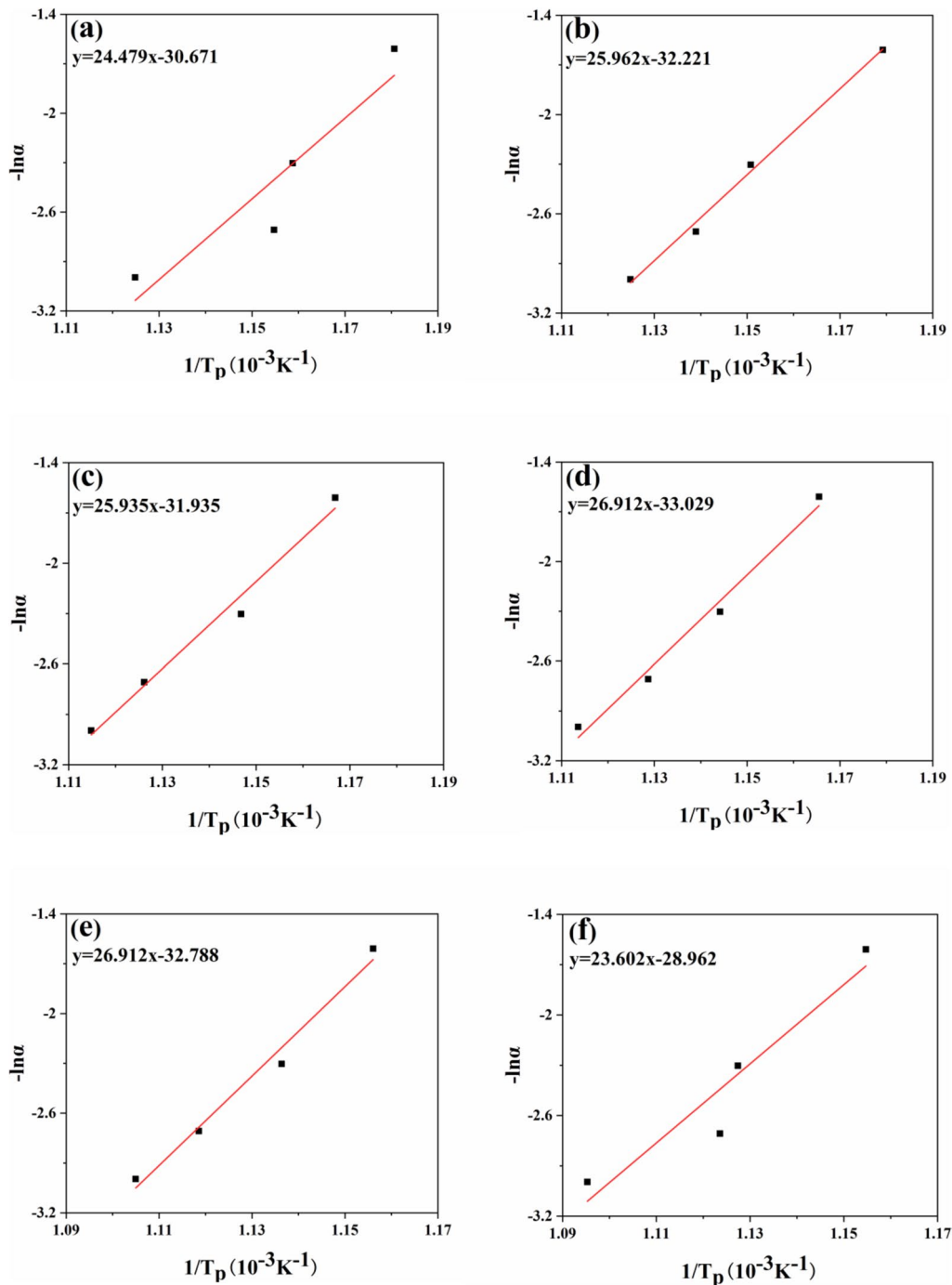
Fig. 3 $-ln\alpha$ vs. $1/T_p$ of glasses with different MnO_2-doping (a-f): a: 0, b: 2%, c: 4%, d: 6%, e: 8%, f: 10%

the other hand, it controls the diffusion of free ions and inhibits the recombination of the glass network.

The calculation of the crystallization kinetic parameter E_c is shown in Table 2, and the crystallization activation energy is in an overall trend of increasing first and then decreasing, at the beginning, the content of Mn is small, and the proportion of Si–O–Si is high, when the content of Mn is gradually increased, and the proportion of Si–O-Mn is gradually increased, the stability of Si–O-Mn is not as good as that of Si–O-Si, and the anti-polarization phenomenon occurs, which promotes the precipitation of crystals. In summary, Mn in glass–ceramics, when the content is low, inhibit grain growth, grain refinement; when the content is high, it will promote the nucleation and crystallization of glass–ceramics.

Crystallization tendency of glass–ceramics

Figure 4 is the Raman spectra of glass–ceramics doped with different contents of MnO_2 slag, which can be roughly divided into two parts: the first part is located at 600-800 cm^{-1}, which represents the low frequency band of the characteristic vibration mode of the network structure unit in the glass network; the second part is the high frequency band representing the network connectivity, which is located in the 800-1200 cm^{-1} band. In the low frequency band, the intensity of the vibration peak increases first and then decreases with the increase of MnO_2, which represents that different contents of MnO_2 have different effects on the glass network. In the high frequency band, the peak area of different Q^n structural units in the glass sample was obtained by using the Gaussian deconvolution method for the peak fitting of the 800-1200 cm^{-1} wavenumber Raman peak. The results are shown in Fig. 5.

According to previous studies [27–30], the degree of polymerization (DOP) is an important parameter for the analysis of glass structure. Mysen found that the characteristic frequencies of monomer (Q^0Si), dimer (Q^1Si), chain (Q^2Si) and sheet (Q^3Si) were 840–860 cm^{-1}, 900–920 cm^{-1}, 960–980 cm^{-1} and 1050 cm^{-1}, respectively.
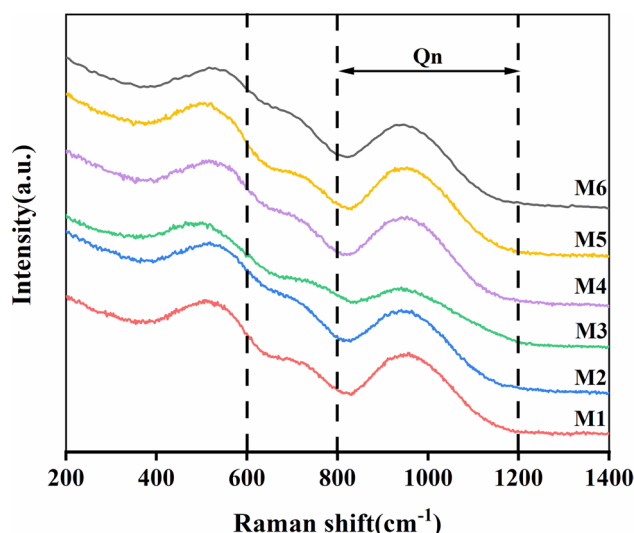

**Fig. 4** Raman spectra of the glass samples and the deconvolution in the range from 100 cm^{-1} to 1900 cm^{-1}

After that, Macmillan summarized the characteristic frequencies of Q^nSi at 850 cm^{-1}, 900 cm^{-1}, 950–1000 cm^{-1}, 1050–1100 cm^{-1} and 1200 cm^{-1}, respectively. In general, the proportion of Q^n unit content is linear with the proportion of characteristic peak area. DOP was determined by the following formula [31]. The results are shown in Table 3.

$$BO/T = 4 \times Q^4 + 3 \times Q^3 + 2 \times Q^2 + 1 \times Q^1 + 0 \times Q^0 \quad (7)$$

It can be seen from Table 3 that the content of Q^2 increases first and then decreases, which indicates that in the silicate network, with the increase of manganese content, the $[MnO_4]$ tetrahedron is gradually formed in the network structure, and the structure needs Na^+ and other metal cations to neutralize its electricity to make it stable. Therefore, the concentration of metal cations around the $[SiO_4]$ tetrahedron decreases, and the content of bridge oxygen bonds increases accordingly. The process of ion diffusion is inhibited, which hinders the process of crystal

Table 2 Glass stability (K_{GS}), Activation energy (E_c) and Avrami parameters (n)

Sample Number		M1	M2	M3	M4	M5	M6
K_{GS}		0.4	0.43	0.44	0.41	0.41	0.44
Crystallization temperature T_p (℃)	α=5 ℃/min	847	848	857	858	865	866
	α=10 ℃/min	863	869	872	874	880	887
	α=15 ℃/min	866	878	888	886	894	890
	α=20 ℃/min	889	889	897	898	905	913
Activation energy E_c (kJ/mol)	Kissinger method	326.24	348.22	345.70	359.45	357.89	309.67
	Ozawa-Matusita method	351.35	373.33	370.90	351.42	383.22	335.10
Avrami parameter n	α=10 ℃/min	0.8	0.9	1.1	0.6	0.6	0.8
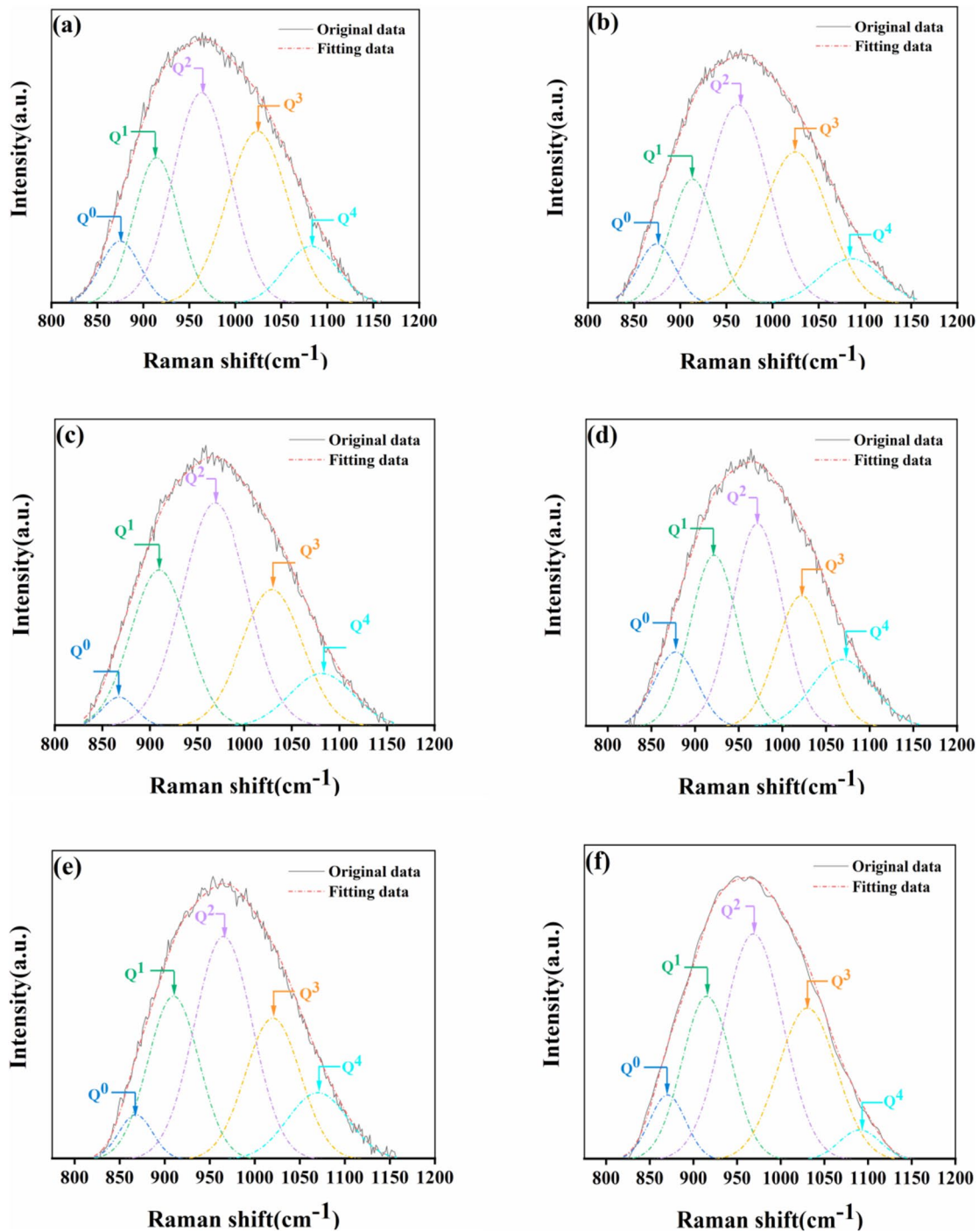
Fig. 5 Doconvoluted Raman spectra in the range from 800 cm^{-1} to 1200 cm.$^{-1}$. (a) – M1, (b) – M2, (c) – M3, (d) – M4, (e) – M5, (f) – M6

nucleation and grain growth. When MnO_2 is added to a certain extent, Si–O-Mn dominates, which is not as stable as Si–O-Si, as a result, the content of Q^2 decreased. However, after comprehensive analysis with Q^0, Q^1, Q^3 and Q^4, The DOP of glass–ceramics generally tends to increase and then decrease. Therefore, the addition of a small amount of

manganese can promote the glass network to become more stable. At this time, it is difficult for ions to diffuse to the corresponding positions in the lattice, leading to an increase in the difficulty of crystallisation. However, an excess of manganese promotes the diffusion of particles, in agreement with the conclusion of DSC.

Table 3 Fitting results for Q_n and calculation of BO/T

Sample	Q^0	Q^1	Q^2	Q^3	Q^4	BO/T (DOP)	R^2
M1	51,755.86	138,074.59	252,590.05	221,398.52	63,702.76	2.15	0.99719
M2	55,534.87	141,770.77	308,892.86	250,968.96	69,268.77	2.16	0.99791
M3	20,514.24	189,719.56	313,772.43	180,029.58	71,328.82	2.12	0.99747
M4	67,103.16	170,831.90	214,255.64	137,677.93	86,436.05	2.01	0.99764
M5	55,853.80	134,625.87	362,974.36	173,899.91	59,678.67	2.05	0.99763
M6	47,774.18	165,676.27	276,320.16	182,035.06	25,327.83	1.96	0.99936
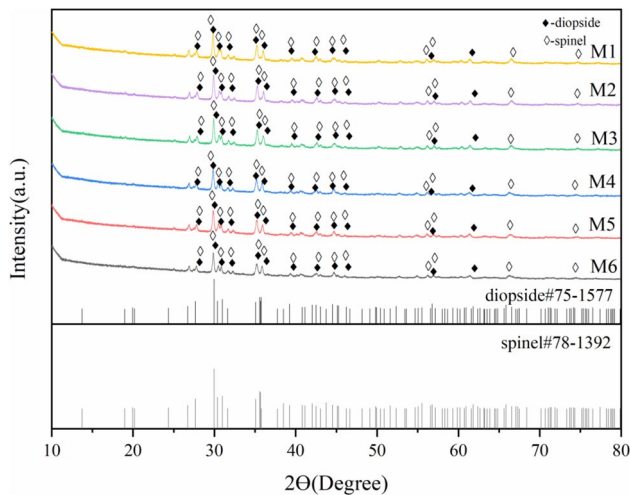
Fig. 6 XRD pattern of glass–ceramics with different MnO_2-doping: M1: 0, M2: 2%, M3: 4%, M4: 6%, M5: 8%, M6:10%

## Effect on the structure of glass–ceramics glass

Figure 6 shows the X-ray diffraction results of glass samples M1-M6 crystallized at 860 °C for 2 h. As shown in the figure, the main crystal phase of the glass is diopside, and the second phase is spinel. The intensity of the diffuse scattering peak at about 30° decreases with the increase of MnO_2 addition, and the diffraction peak gradually shifts to the left, indicating that the crystallization tendency of diopside decreases. The reason for this phenomenon may be that Mn^{4+} with larger ionic radius replaces Si^{4+} with smaller ionic radius in the crystal phase to form a $[MnO_4]$ tetrahedron, which accumulates with the surrounding tetrahedron, hinders the diffusion of other ions, and inhibits the formation of diopside.

During the melting process, MgO and Cr_2O_3 preferentially form Mg-Cr spinel to induce the epitaxial growth of diopside and act as nucleating agents for heterogeneous nucleation. At the same time, after Mn^{4+} enters the glass network, it will break the original stable silicon-oxygen tetrahedron structure and release more free oxygen. At this time, the octahedron $[MgO_6]^{10-}$, $[SiO_3]^{2-}$ and $[CaO_6]^{10-}$ are combined into diopside in the form of double chains. Therefore, we believe that Mn^{4+} is supersaturated in spinel and then enters the diopside structure in an enriched state. Because the iron in the tailings can be used as an effective nucleating agent, the initial nucleation of glass–ceramics can produce magnetite phase, and the iron-rich region evenly distributed in the glass–ceramics matrix can be used as the nucleation center, which greatly promotes the formation and growth of the diopside phase, so the diffraction peak gradually shifts to the left is not obvious.

In summary, although Mn^{4+} has a certain effect on delaying crystallization, it does not participate in the formation of the main crystal phase, so it has no obvious effect on the type of the main crystal phase.

Figure 7 shows the effect of adding MnO_2 on the surface morphology of the glass–ceramics. As seen from the image, the glass–ceramics grows tiny crystals dominated by spherical crystals, on the one hand, the Avrami index n of the glass is close to 1 (Table 2), and the crystals can't grow up; on the other hand, there are a large number of nucleation agents such as iron oxide in the tailings, and sufficient nucleation agents ensure the nucleation and crystallization of glass–ceramics during heat treatment. MnO_2 mainly exists in the glassy phase and does not participate in the formation of the main crystalline phase, so it has no significant effect on the morphology of the crystals, which is also proved by the XRD results. Among them, the cracks in the M1-M4 samples are dense and irregular, while in the M5 and M6 samples the density of the cracks is significantly reduced, and irregular clusters are produced, so that the cracks are deflected or interrupted when encountering clusters in the process of expansion. The Mn^{4+} studied in this paper occupies a tetrahedral position in the glass and exists in the form of a network forming body, as well Mn^{4+} has high field strength, high coordination number and strong aggregation, Mn^{4+} seizes non-bridging oxygen in the form of $[MnO_4]$ tetrahedral coordination form to participate in the formation of silica-oxygen network. The existence of clusters makes cracks in the process of expansion is hindered, the consumption of cracking energy, thus inhibiting the crack expansion and achieve the effect of strengthening the glass–ceramics.
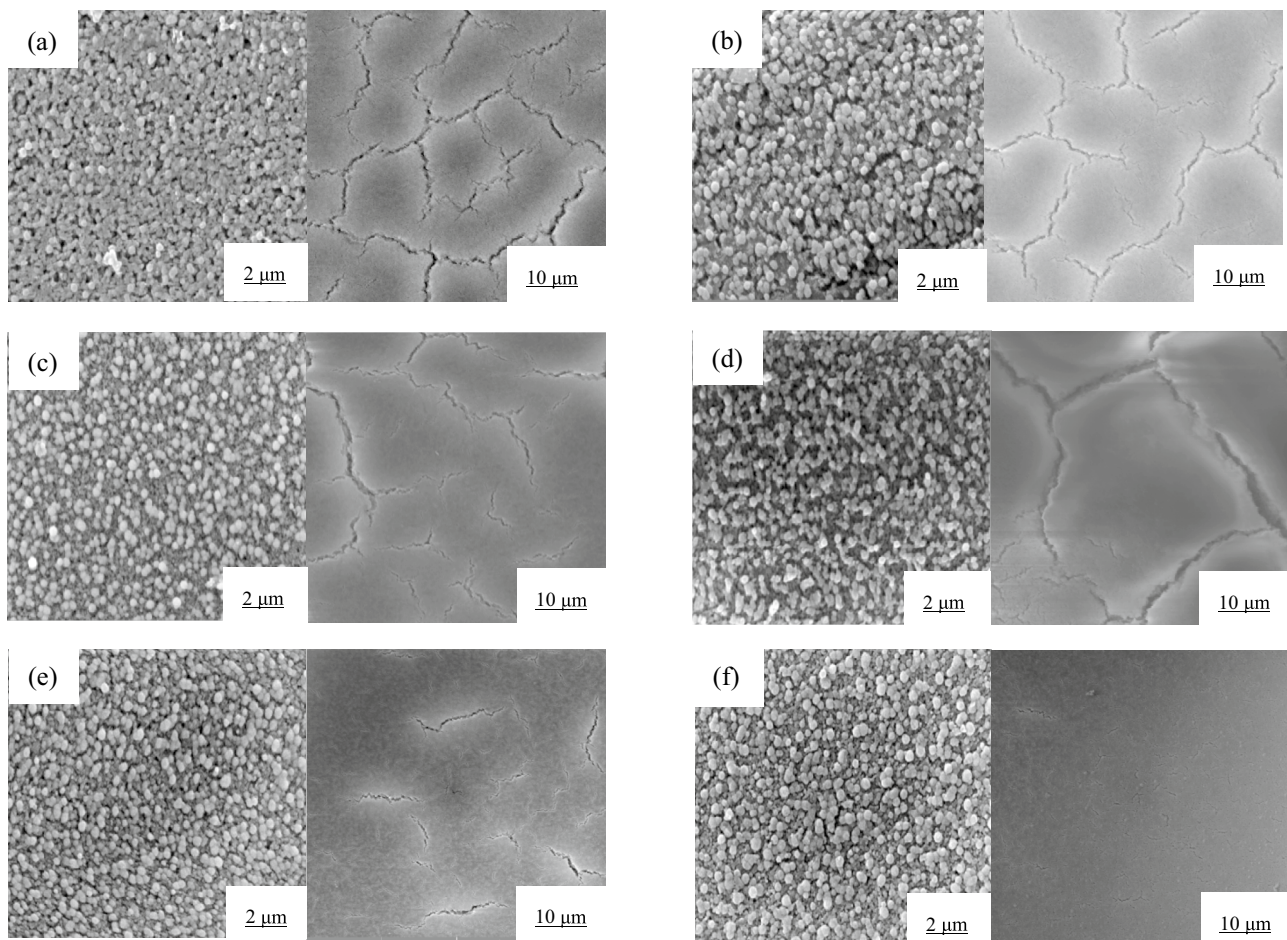
Fig. 7 SEM images of the different MnO_2 content glass–ceramics crystallized at the heating rate of 10 °C/min. (a) 0% MnO_2; (b) 2% MnO_2; (c) 4% MnO_2; (d) 6% MnO_2; (e) 8% MnO_2; (f) 10% MnO_2. Left: high magnification; right: low magnification

Conclusion

CaO-MgO-Al_2O_3-SiO_2(CMAS) glass–ceramics with MnO_2 addition were prepared by conventional melting method. Through the characterization test of crystallization kinetics and microstructure of glass–ceramics, the following conclusions can be drawn:

1. The addition of MnO_2 to the diopside glass–ceramics can improve the degree of polymerization of the initial phase glass–ceramics, enhance the stability of the glass structure, and increase the crystallization temperature of the diopside phase.
2. The addition of MnO_2 does not change the main crystalline phase of
3. CaO-MgO-Al_2O_3-SiO_2(CMAS) glass–ceramics, but improves the integrity and compactness of the glass network to a certain extent, and reduces the crystalliza-

tion tendency of the glass network, thus weakening the crystallization characteristics of the glass–ceramics.
4. The addition of MnO_2 has an inhibitory effect on the crack propagation behavior in glass ceramics, which is mainly related to the characteristics of high field strength and high coordination number of Mn^{4+} ions and aggregates.

Data Availability The authors confirm that the data supporting the findings of this study are available within the article. Data is available upon the Manager's approval.

Declarations

Competing Interest There is no conflict of interest with this work.

References

1. Wang, Z., Sohn, I.: Understanding the solidification and leaching behavior of synthesized Cr-containing stainless steel slags with varying Al_2O_3/SiO_2 mass ratios. J. Ceram. Int. **47**(8), 10918-10926 (2021)

2. Song, W., Zhu, Z., Cao, J., et al.: Core-shell microstructure simultaneous solidification mechanism of Cr(III), Mn(IV), Ni(II) and Pb(II) in glass-ceramics. J. J. Non-Cryst. Solids. **563**, 120809 (2021)

3. Li, J.Y.S.A.: Removal and immobilization of heavy metals in contaminated soils by chlorination and thermal treatment on an industrial-scale. J. Chem. Eng. J. **359**, 389–392 (2019)

4. Christian, A.: Heavy metal removal from sewage sludge ash by thermochemical treatment with polyvinylchloride. J. Environ. Sci. Technol.: ES&T. **47**(1), 563–567 (2013)

5. Zhang, F.S., Itoh, H.: Extraction of metals from municipal solid waste incinerator fly ash by hydrothermal process. J. J. Hazard. Mater. **136**(3), 663–670 (2006)

6. Sun, Z., Xiao, Y., Sietsma, J., et al.: A cleaner process for selective recovery of valuable metals from Electronic Waste of Complex Mixtures of End-of-Life Electronic Products. J. Environ. Sci. Technol. **49**(13), 7981–7988 (2015)

7. Oliveira, J.A., Cunha, F.A., Ruotolo, L.: Synthesis of zeolite from sugarcane bagasse fly ash and its application as a low-cost adsorbent to remove heavy metals. J. Clean. Prod. **229**, 956–963 (2019)

8. Klein, T.Y., Wehling, J., Treccani, L., et al.: Effective bacterial inactivation and removal of copper by porous ceramics with high surface area. J. Environ. Sci. Technol. **47**(2), 1065–1072 (2013)

9. Funari, V., Mäkinen, J., Salminen, J., et al.: Metal removal from Municipal Solid Waste Incineration fly ash: A comparison between chemical leaching and bioleaching. J. Waste Manag. **60**, 397–406 (2017)

10 Liao, C., Tang, Y., Liu, C., et al.: Double-Barrier mechanism for chromium immobilization: A quantitative study of crystallization and leachability. J. J. Hazard. Mater. **311**, 246–253 (2016)

11. Liu, L., Yu, H., Li, Y., et al.: Stabilization behavior and mechanism of heavy metals in eco-friendly glass-ceramics derived from wastes. J. J. Clean. Prod. **269**(8), 122417 (2020)

12 Pan, D.A., Li, L.J., et al.: Production of glass-ceramics from heavy metal gypsum and pickling sludge. J. Int. J. Environ. Sci. Technol. **12**(9), 3047–3052 (2015)

13. Song, W., Cao, J., Wang, Z., et al.: Glass-ceramics microstructure formation mechanism for simultaneous solidification of chromium and nickel from disassembled waste battery and chromium slag. J. J. Hazard. Mater. **403**, 123598 (2020)

14. Stoch, P., Ciecińska, M., Stoch, A., et al.: Immobilization of hospital waste incineration ashes in glass-ceramic composites. J. Ceram. Int. **44**(1), 728–734 (2017)

15. Chen, H,.H., Lin,H.R.,et al.: Immobilisation of heavy metals in hazardous waste incineration residue using SiO_2-Al_2O_3-Fe_2O_3-CaO glass-ceramic. Ceram. Int. **47**(6), 8468-8477 (2021)

16. Dai, C.L., Yang, Y., Yang, M.: The role and influence of manganese in architectural ceramic glaze and glass-ceramics. J. Foshan Ceram. **8**, 40–42 (2011)

17. Abdel-Hameed, S.A.M., Marzouk, M.A., Farag, M.M.: Effect of P_2O_5 and MnO_2 on crystallization of magnetic glass ceramics. J. J. Adv. Res. **5**(5), 543–550 (2014)

18 Wang, X.R., Zhang, Y., Ma, T., et al.: Effects of MnO_2 concentration on dielectric properties of barium strontium titanate glass ceramics. J. Ceram. Int. **38**(supp-S1), S57–S60 (2012)

19. Li, B., Deng, L., Zhang, X., et al.: Structure and performance of glass-ceramics obtained by Bayan Obo tailing and fly ash. J. J. Non-Cryst. Solids. **380**, 103–108 (2013)

20. Deng, L., Wang, S., Zhang, Z., et al.: The viscosity and conductivity of the molten glass and crystallization behavior of the glass ceramics derived from stainless steel slag. J. Mater. Chem. Phys. **251**, 123159 (2020)

21. Jiusti, J., Cassar, D.R., Zanotto, E.D.: Which glass stability parameters can assess the glass-forming ability of oxide systems? J. Int. J. Appl. Glas. Sci. **11**(4), 612–621 (2020)

22. Saad, M., Poulain, M.,: Glass forming ability criterion. J. Mater. Sci. Forum. **163**, 19–20 (1987)

23. Kissinger, H.E.: Variation of Peak Temperature With Heating Rate in Differential Thermal Analysis. J. J. Res. Natl. Bur. Stand. **57**(4), 217–221 (1956)

24. Augis, J.A., Bennett, J.E.: Calculation of the Avrami parameters for heterogeneous solid state reactions using a modification of the Kissinger method. J. J. Therm. Anal. **13**(2), 283–292 (1978)

25. Cheng, K., Wan, J.: Study on the crystallization kinetics of mica glass- ceramics. J. J. Chin. Ceram. Soc. **25**(5), 6 (1997)

26. Zhang, Y., Liu, X., Xu, Y., et al.: Preparation of road base material by utilizing electrolytic manganese residue based on Si-Al structure: Mechanical properties and Mn^{2+} stabilization/solidification characterization. J. J. Hazard. Mater. **390**, 122188 (2020)

27. Ouyang S L, Zhang, Y X., Chen, Y X, et al.: Preparation of Glass-ceramics Using Chromium-containing Stainless Steel Slag: Crystal Structure and Solidification of Heavy Metal Chromium. J. Sci. Rep. **9**(1), 1–9 (2019)

28. Bjorn, MYSEN. Physics and chemistry of silicate glasses and melts. J. Eur. J. Mineral. **15**(5), 781–802 (2003)

29 Sohn, I., Min, D.J.: A review of the relationship between viscosity and the structure of Calcium-Silicate-Based Slags in Ironmaking. J. Steel Res. Int. Int. **83**(7), 611–630 (2012)

30. Zhang, Y. L., Zhuo, Q., et al. Viscosity measurement and structure analysis of Cr_2O_3-Bearing CaO-SiO_2-MgO-Al_2O_3 Slags. J. Metall. and Mater. Trans, B. Process Metall Mater Process. Sci. 48B(1),346–356 (2017)

31. Zhao, S., Liu, B., Ding, Y., et al.: Study on glass-ceramics made from MSWI fly ash, pickling sludge and waste glass by one-step process. J. J. Clean. Prod. **271**, 122674 (2020)